Supporting Information

Novel Nitrogen-Containing Heterocyclic Non-Fullerene Acceptors for Organic Photovoltaic Cells: Different End-capping Group Leading to Big Difference of Power Conversion Efficiencies

Guanghao Li,[ab,#] Chunyu Xu,[c,#] Zhenghui Luo,[a] Weimin Ning,[a] Xiaohui Liu,[b] Shaolong Gong,[a] Yang Zou,[b] Fujun Zhang,*[c] Chuluo Yang*[ab]

[a] Hubei Key Lab on Organic and Polymeric Optoelectronic Materials, Department of Chemistry, Wuhan University, Wuhan 430072, China. E-mail: clyang@whu.edu.cn

[b] Shenzhen Key Laboratory of Polymer Science and Technology, College of Materials Science and Engineering, Shenzhen University, Shenzhen 518060, China.

[c] Key Laboratory of Luminescence and Optical Information, Ministry of Education, Beijing Jiaotong University, Beijing 100044, China. E-mail: fjzhang@bjtu.edu.cn

# These authors contributed equally to this work.

Instruments and Measurements

^{1}H NMR (400 MHz) and ^{13}C NMR (100 MHz) spectra were measured on a MERCURYVX300 spectrometers. HR-ESI-MS was recorded on a Thermo Scientific LTQ Orbitrap XL mass spectrometer. UV-vis-NIR absorption spectra were recorded on a Shimadzu UV-2501 recording spectrophotometer. Cyclic voltammetry (CV) measurements were carried out on a CHI voltammetry analyzer at room temperature. Tetrabutylammonium hexafluorophosphate (*n*-Bu4NPF6, 0.1 M) was used as the supporting electrolyte. The conventional three-electrode configuration consists of a

platinum working electrode with a 2 mm diameter, a platinum wire counter electrode, and an Ag/AgCl wire reference electrode. Cyclic voltammograms were obtained at a scan rate of 100 mV/s. PL spectra were measured with a Shimadzu RF-5301PC fluorescence spectrophotometer. Instrument Parameters : Measurement type: Wavelength scan; Scan mode: Emission; Data mode: Fluorescence; Scan speed: 240 nm/min; EX Slit: 5.0 nm, EM Slit: 5.0 nm; PMT Voltage: 400 V. PL quenching was calibrated for the film absorption at the excitation wavelength, and the PL quenching efficiency was estimated from the ratio of the PL intensity of polymer: acceptors film sample to that of the polymer or acceptors control sample. DFT calculations were performed by using Gaussian at the B3LYP/6-311G(d,p) level, and the long alkyl chains was simplified as methyl. The film morphology was measured using an atomic force microscope (AFM, Bruker-ICON2-SYS) using the tapping mode. The RMS values of the surface AFM images are averaged based on five times testing on different areas for each sample. TEM images were performed on a JEOL JEM-1400 transmission electron microscope.

Device Fabrication and Characterization

The PSCs were fabricated with a structure of ITO/PEDOT: PSS (30 nm)/active layer/cathode. A thin layer of PEDOT: PSS was deposited through spin-coating on precleaned ITO-coated glass from a PEDOT: PSS aqueous solution (Baytron P VP AI 4083 from H. C. Starck) at 2000 rpm and dried subsequently at 150 °C for 15 minutes in air. Then the device was transferred to a nitrogen glove box, where the active blend layer of PM6 polymer and BDTN-BF (or BDTN-Th) was spin-coated from its chloroform solution onto the PEDOT: PSS layer under a spin-coating rate of 2500 rpm. After spin-coating, the active layers were annealed at 80 °C for 5 minutes for the devices with thermal annealing treatment. The thickness of the active layers is ca. 145

nm. Then methanol solution of PDINO at a concentration of 1.0 mg mL^{-1} was deposited atop the active layer at 3000 rpm for 30 s to afford a PDIN cathode buffer layer with thickness of ca. 10 nm. Finally, top Al electrode was deposited in vacuum onto the cathode buffer layer at a pressure of ca. 5.0×10^{-5} Pa. All film thickness was measured by the Alpha-Step D-500 surface profilometer. The current density-voltage (J-V) characteristics of the PSCs were measured in glovebox on a computer-controlled Keithley 2450 Source-Measure Unit. Oriel Sol3A Class AAA Solar Simulator (model, Newport 94023A) with a 450 W xenon lamp and an air mass (AM) 1.5 filter was used as the light source. The light intensity was calibrated to 100 Mw cm^{-2} by a Newport Oriel 91150V reference cell. The input photon to converted current efficiency (EQE) was measured by Solar Cell Spectral Response Measurement System QE-R3-011 (Enli Technology Co., Ltd., Taiwan). The light intensity at each wavelength was calibrated with a standard single-crystal Si photovoltaic cell. Optical microscope (Olympus BX51) was used to defined the active area (4.6 mm^2) of the device. Masks made using laser beam cutting technology to have a well-defined area of 2.2 mm^2 were attached to define the effective area for accurate measurement. All the masked and unmasked tests gave consistent results with relative errors within 0.5%. The J_{SC} values obtained by integrating the product of the EQE with the AM 1.5G solar spectrum agreed with the measured value to within 3%. All the device measurements were undertaken in a nitrogen glovebox (O_2 < 0.1 ppm, H_2O < 0.1 ppm). For the *J–V* measurement, the voltage step and delay time were 10 mV and 1 ms, respectively. The scan started from -1.5 V to 1.5 V.

Mobility Measurements

Hole and electron mobility were measured using the space charge limited current

(SCLC) method. Device structures are ITO/PEDOT: PSS/BHJs (1:1, w/w) /Au for hole-only devices and ITO/ZnO/ BHJs (1: 1, w/w)/PDIN/Al for electron-only devices. The SCLC mobilities were calculated by MOTT-Gurney equation:

$$J = 9\varepsilon_0\varepsilon_r\mu V^2/8d^3$$

Where J is the current density, ε_r is the relative dielectric constant of active layer material usually 2-4 for organic semiconductor, herein we use a relative dielectric constant of 3, ε_0 is the permittivity of empty space (8.85×10^{-12} F m^{-1}), μ is the mobility of hole or electron and d is the thickness of the active layer, V is the internal voltage in the device, and $V = V_{Applied} - V_{Built\text{-}in}$ (in the hole-only and the electron-only devices, the V_{bi} values are 0.2 V and 0 V respectively), where $V_{Applied}$ is the voltage applied to the device, and $V_{Built\text{-}in}$ is the built-in voltage resulting from the relative work function difference between the two electrodes.

Experimental Section

All solvents and reagents were used as received from commercial sources and used without further purification unless otherwise specified. Compound 2-4 were synthesized according to reported methods.[1-3] Compound BDTN, BDTN-CHO, BDTN-BF and BDTN-Th were synthesized as follows:

Compound **BDTN**. A mixture of compound 4 (370 mg, 0.4 mmol), sodium tert-butoxide (300 mg, 3.1 mmol), $Pd_2(dba)_3$ (46 mg, 0.05 mmol) and 1,1´-bis(diphenylphosphino)ferrocene (dppf, 55 mg, 0.1 mmol) in anhydrous toluene (5 mL) was stirred at room temperature for 10 minutes. To the resulting solution was then added 2-butyloctylamine (170 mg, 0.9 mmol) in 1 ml of anhydrous toluene and the

mixture was stirred at 120 °C for 2 h. After cooling to room temperature, H_2O was added to the resulting mixture and extracted with CH_2Cl_2 three times. The combined organic layer was dried over $MgSO_4$ and concentrated under reduced pressure. The residue was purified by column chromatography on silica gel using petroleum ether/dichloromethane (9:1, v/v) as eluent to obtain BDTN as the viscous yellow oil (155 mg, 40% yield). ^{1}H NMR ($CDCl_3$, 400 MHz): δ [ppm]: 7.19 (d, J = 5.2 Hz, 2H), 7.09 (d, J = 5.3 Hz, 2H), 4.70 (d, J = 7.6 Hz, 4H), 4.15 (t, J = 6.8 Hz, 4H), 2.01-1.93 (m, 6H), 1.62-1.58 (m, 8H), 1.42-1.38 (m, 8H), 1.34-1.31 (m, 8H), 1.25-1.20 (m, 4H), 1.12-1.02 (m, 24H), 0.91 (t, J = 7.0 Hz, 6H), 0.77 (t, J = 7.0 Hz, 6H), 0.69 (t, J = 7.1 Hz, 6H). ^{13}C NMR (100 MHz, $CDCl_3$): δ [ppm]: 146.42, 142.72, 136.94, 133.84, 123.70, 119.31, 115.82, 114.36, 112.14, 74.30, 52.39, 38.57, 31.89, 31.64, 31.60, 30.71, 30.44, 29.66, 29.48, 29.43, 29.31, 29.06, 28.10, 28.06, 26.06, 25.87, 25.85, 22.87, 22.80, 22.69, 22.67, 22.54, 14.15, 14.06, 13.85. HR-ESI-MS (m/z): calcd for $C_{58}H_{89}N_2O_2S_4^+$ $(M+H)^+$ 973.58014, found 973.57904.

Compound **BDTN-CHO**. DMF (10 mL) was slowly injected into phosphorus oxychloride (2.5 mL) at 0 °C. After stirring for 2 hours, compound BDTN (300 mg, 0.3 mmol) in 1,2-dichloroethane (25 mL) was added. The mixture was refluxed at 65 °C for 12 h, then the reaction was quenched with aqueous sodium succinate, and extracted with dichloromethane. After removing the solvent from filtrate, the residue was purified by column chromatography on silica gel using petroleum ether/dichloromethane (2:1, v/v) as eluent to obtain BDTN-CHO as the deep orange solid (240 mg, 75% yield). ^{1}H NMR ($CDCl_3$, 400 MHz): δ [ppm]: 9.94 (s, 2H), 7.72 (s, 2H), 4.75 (d, J = 7.7 Hz, 4H),

4.18 (t, J = 6.8 Hz, 4H), 2.02-1.95 (m, 6H), 1.62-1.59 (m, 8H), 1.42-1.39 (m, 8H), 1.34-1.31 (m, 8H), 1.21-1.19 (m, 4H), 1.13-1.05 (m, 24H), 0.91 (t, J = 7.1 Hz, 6H), 0.76 (t, J = 7.0 Hz, 6H), 0.70 (t, J = 7.0 Hz, 6H). ^{13}C NMR (100 MHz, $CDCl_3$): δ [ppm]: 183.11, 145.83, 143.74, 141.47, 141.41, 135.44, 123.48, 120.59, 119.74, 115.56, 74.99, 52.71, 38.91, 36.08, 34.68, 31.89, 31.62, 30.71, 30.43, 29.73, 29.64, 29.48, 29.45, 29.30, 29.08, 28.09, 26.04, 25.83, 22.88, 22.83, 22.69, 22.65, 22.55, 14.17, 14.06, 13.86, 11.48. HR-ESI-MS (m/z): calcd for $C_{60}H_{88}N_2O_4S_4^+$ $(M+H)^+$ 1028.56214, found 1028.56264.

Compound **BDTN-BF**. BDTN-CHO (110 mg, 0.1 mmol) and 2-(5,6-difluoro-3-oxo-2,3-dihydro-1H-inden-1-ylidene)malononitrile (70 mg, 0.3 mmol) were added to a 25 ml two-necked flask. After being flushed by a gentle stream of dry nitrogen for 15 min, chloroform (10 ml) was added and the two compounds were fully dissolved by stirring for a while. Then pyridine (0.6 ml) was added and the mixture was refluxed at 65 °C for 12 hours. After most of the solvent was evaporated, the crude product was washed by methanol. The residue was purified by column chromatography with petroleum ether/dichloromethane (3:2, v/v) as the eluent to obtain BDTN-BF as the dark blue solid (90% yield). ^{1}H NMR ($CDCl_3$, 400 MHz): δ [ppm]: 8.92 (s, 2H), 8.47 (m, J = 7.6 Hz, 2H), 7.87 (s, 2H), 7.68 (m, J = 7.5 Hz, 2H), 4.76 (d, J = 7.6 Hz, 4H), 4.24 (t, J = 6.9 Hz, 4H), 2.04-2.01 (m, 6H), 1.66-1.59 (m, 8H), 1.46-1.41 (m, 8H), 1.37-1.35 (m, 8H), 1.24-1.20 (m, 4H), 1.12-1.08 (m, 24H), 0.94 (t, J = 7.0 Hz, 6H), 0.76 (t, J = 6.9 Hz, 6H), 0.72 (t, J = 7.1 Hz, 6H). ^{13}C NMR (100 MHz, $CDCl_3$): δ [ppm]: 185.79, 158.44, 155.43, 153.01, 152.86, 148.04, 145.17, 144.72, 138.77, 137.15, 136.86, 136.38, 134.40, 132.41, 126.97, 120.55, 120.14, 117.08, 114.85, 114.59, 112.58,

112.40, 75.60, 68.20, 53.08, 38.85, 31.87, 31.61, 30.62, 30.43, 30.35, 29.65, 29.49, 29.33, 28.01, 26.07, 25.76, 22.88, 22.70, 22.54, 14.17, 14.05, 13.84. HR-ESI-MS (m/z): calcd for $C_{84}H_{92}F_4N_6O_4S_4^+$ $(M)^+$ 1452.59935, found 1452.59851.

Compound **BDTN-Th**. BDTN-CHO (110 mg, 0.1 mmol) and 2-(6-oxo-5,6-dihydro-4H-cyclopenta[c]thiophen-4-ylidene)malononitrile (60 mg, 0.3 mmol) were added to a 25 ml two-necked flask. After being flushed by a gentle stream of dry nitrogen for 15 min, chloroform (10 ml) was added and the two compounds were fully dissolved by stirring for a while. Then pyridine (0.6 ml) was added and the mixture was refluxed at 65 °C for 12 hours. After most of the solvent was evaporated, the crude product was washed by methanol. The residue was purified by column chromatography with petroleum ether/dichloromethane (3:2, v/v) as the eluent to obtain BDTN-Th as the dark blue solid (90% yield). ^{1}H NMR ($CDCl_3$, 400 MHz): δ [ppm]: 8.89 (s, 2H), 8.36 (d, J = 2.3 Hz, 2H), 7.94 (d, J = 2.2 Hz, 2H), 7.88 (s 2H), 4.72 (d, J = 7.7 Hz, 4H), 4.21 (t, J = 6.8 Hz, 4H), 2.04-1.97 (m, 6H), 1.66-1.63 (m, 8H), 1.48-1.42 (m, 8H), 1.37-1.33 (m, 8H), 1.26-1.21 (m, 4H), 1.13-1.09 (m, 24H), 0.93 (t, J = 6.9 Hz, 6H), 0.76 (t, J = 6.9 Hz, 6H), 0.71 (t, J = 7.0 Hz, 6H). ^{13}C NMR (100 MHz, $CDCl_3$): δ [ppm]: 181.39, 156.59, 148.06, 144.80, 144.58, 142.55, 142.33, 139.95, 137.32, 136.70, 132.30, 127.74, 127.27, 126.59, 125.10, 120.07, 117.02, 115.44, 114.86, 75.51, 66.08, 53.04, 38.80, 31.85, 31.61, 30.60, 30.39, 30.34, 29.61, 29.49, 29.30, 27.98, 26.05, 25.73, 22.89, 22.68, 22.54, 14.16, 14.05, 13.83. HR-ESI-MS (m/z): calcd for $C_{80}H_{92}N_6O_4S_6^+$ $(M+H)^+$ 1392.54988, found 1392.54822.

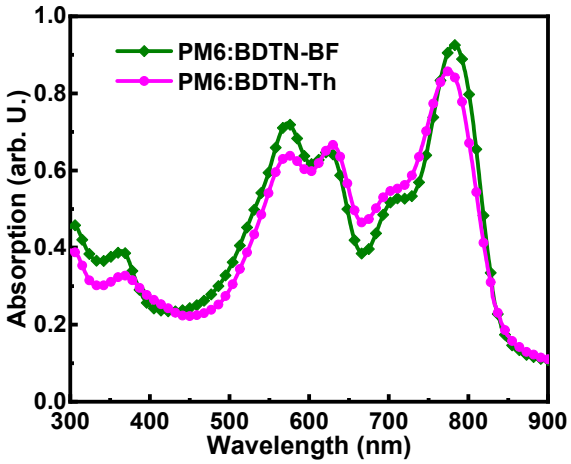

Figure S1. Absorption spectra of PM6:BDTN-BF and PM6:BDTN-Th blend films.

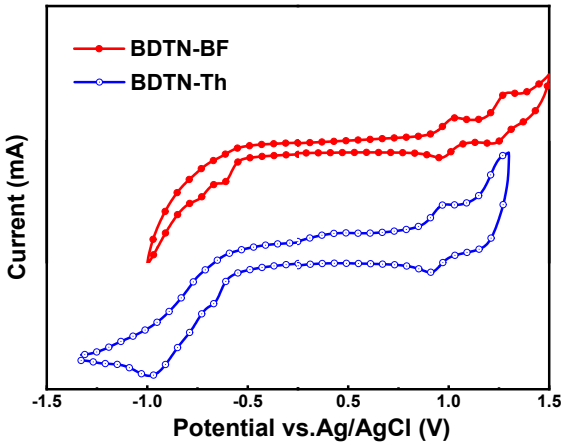

Figure S2. Cyclic voltammograms for BDTN-BF and BDTN-Th films in CH_3CN/0.1 M *n*-Bu4NPF6 at 100 mV s^{-1}, the potential was referred to the Ag/AgCl reference electrode.

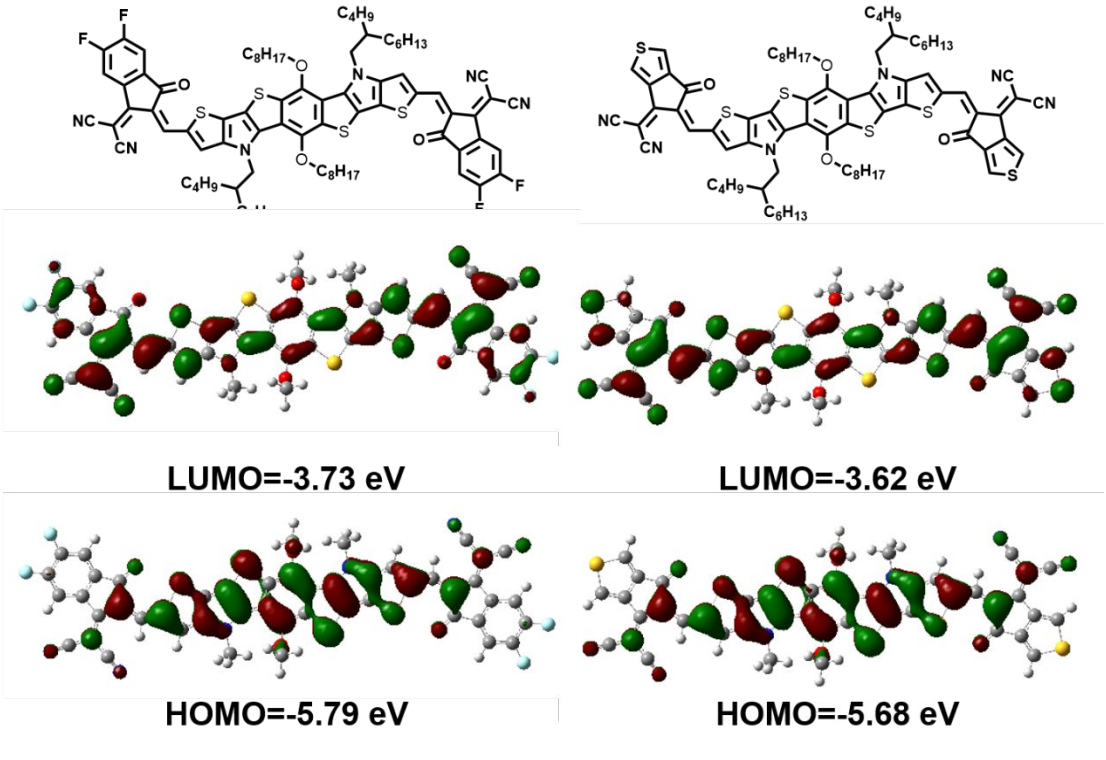

Figure S3. The chemical structures, LUMO and HOMO orbital distributions and energy levels calculated by DFT calculations for BDTN-BF and BDTN-Th.

S_1	Hole	Particle	Transition
BDTN-BF	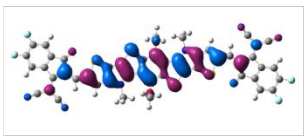	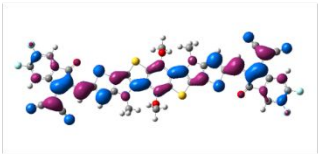	79.1% HOMO-LUMO
BDTN-Th	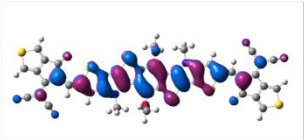	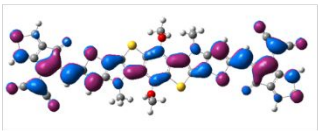	79.9% HOMO-LUMO

Figure S4. The S1 transition of BDTN-BF and BDTN-Th.

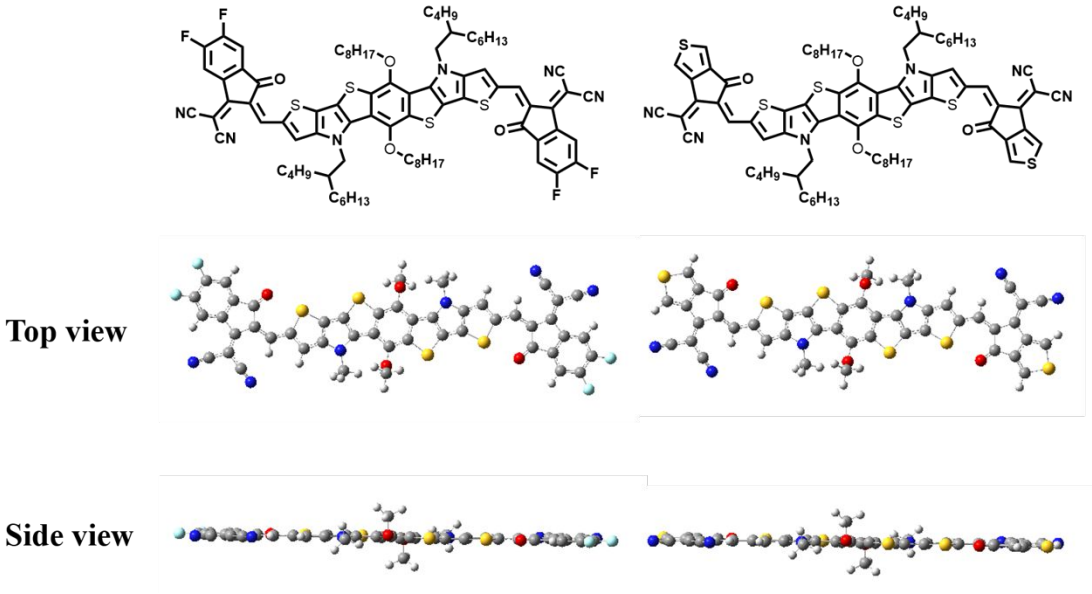

Figure S5. The top and side views of the BDTN-BF and BDTN-Th in optimized molecular geometry.

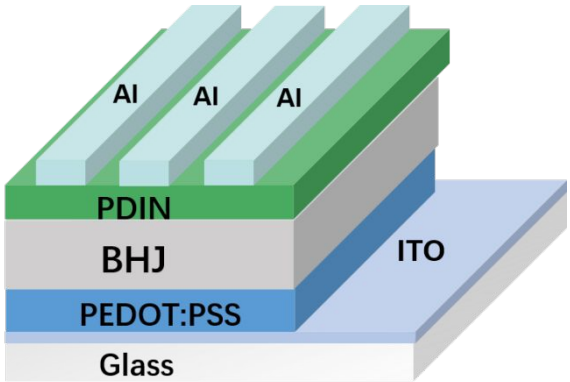

Figure S6. Architecture of BDTN-BF and BDTN-Th based devices.

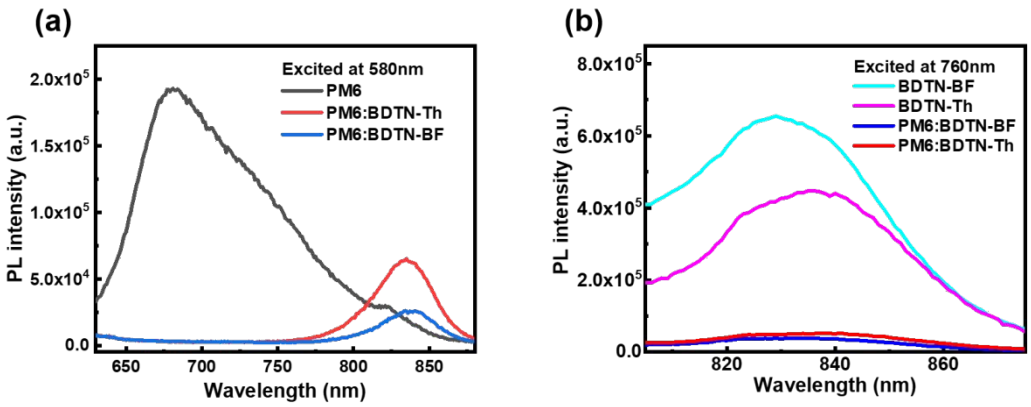

Figure S7. (a) Photoluminescence spectra of the polymer PM6 and the blend films excited at 580 nm; (b) photoluminescence spectra of the acceptors and the blend films excited at 760 nm.

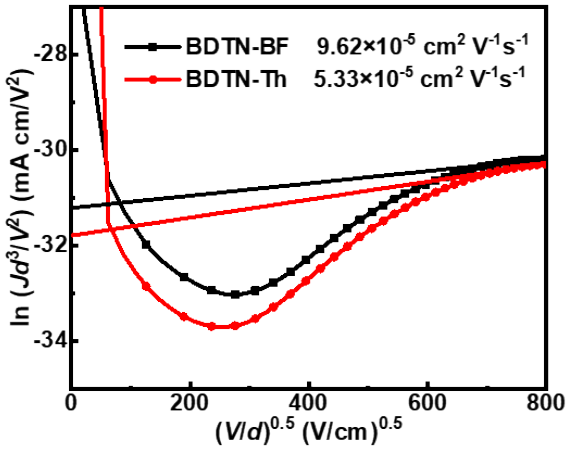

Figure S8. BDTN-BF and BDTN-Th neat films in electron-only devices.

Table S1. Photovoltaic performance of the PSCs based on PM6:BDTN-BF (1:1, w/w) under the illumination of AM 1.5G, 100 mW cm^{-2}.

Treatment	J_{sc} [mA cm^{-2}]	V_{oc} [V]	FF [%]	PCE [%]
As-cast	17.66	0.94	54.28	9.01
TA [a)]	19.07	0.93	54.86	9.73
CS_2 [b)]	19.21	0.92	61.47	10.87
TA [a)] + CS_2 [b)]	20.20	0.93	61.46	11.54

a) Thermal annealing at 80 °C for 5 min.

b) 40 s of CS_2 fumigation.

Table S2. Photovoltaic performance of the PSCs based on PM6:BDTN-Th (1:1, w/w)

under the illumination of AM 1.5G, 100 mW cm^{-2}.

Treatment	J_{sc} [mA cm^{-2}]	V_{oc} [V]	FF [%]	PCE [%]
As-cast	7.62	0.96	42.57	3.13
TA [a)]	8.20	0.95	45.11	3.53
CS_2 [b)]	4.82	0.90	42.56	1.84
TA [a)] + CS_2 [b)]	5.88	0.85	43.40	2.16

a) Thermal annealing at 80 ^{o}C for 5 min.

b) 40 s of CS_2 fumigation.

Table S3. The detailed J_{sc} values of the devices for V_{oc} around 0.93 V.

Devices	V_{oc} [V]	J_{sc} [mA cm^{-2}]	Ref.
J71: m-MeIC	0.922	18.56	4
PBDB-T:BTTIC-TT	0.924	19.61	5
PBDB-T:BTTIC-Ph	0.930	16.47	5
PTQ10:IDTPC	0.93	17.5	6
PBDB-T:MeIC1	0.927	18.32	7
PBT1-C-MW2:ITCPTC	0.93	17.1	8
PBT1-C-HW:ITCPTC	0.93	16.8	8
PBDB-T:BDCPDT-TTC	0.94	17.72	9

PM6:TSeTIC	0.93	19.42	10
PBDB-T:ITBTC	0.941	16.37	11
PBDB-T:IDTO	0.943	16.25	12
PBT1-EH:IDTCN	0.93	13.31	13
PBDB-T:IT-M	0.94	17.44	14
PBT1-C:ITCPTC	0.94	17.0	15

Table S4. The detailed V_{oc} values of the devices for J_{sc} around 20 mA cm^{-2}.

Devices	J_{sc} [mA cm^{-2}]	V_{oc} [V]	Ref.
PBDB-T:BTTIC-Th	19.45	0.902	5
PBDB-T:BTTIC-TT	19.61	0.924	5
PBDB-T:BTTIC	19.52	0.904	16
PM6:ITC-2Cl	20.1	0.91	17
PBDB-T:BTTIC-2M	19.39	0.90	18
PM6:TSeTIC	19.42	0.93	10
FTAZ:IDIC	20.8	0.84	19
PBDB-T:NCBDT	20.33	0.84	20
PBDB-T:NITI	20.67	0.86	21
FTAZ:IOIC2	19.7	0.90	22

PBDB-T:ZITI	19.8	0.89	23
PBDB-T-SF:IT-4F	20.50	0.88	24
PDTB-ET-T:IT-4F	20.73	0.90	25
PBDB-T:IDTOT2F	20.87	0.85	26

Table S5. The data of photocurrent versus the effective voltage of the PM6:BDTN-BF and PM6:BDTN-Th based devices.

Devices	J_{sat} [mA cm^{-2}]	J_{ph}^{a} [mA cm^{-2}]	J_{ph}^{b} [mA cm^{-2}]	J_{ph}^{a}/ J_{sat} [%]	J_{ph}^{b}/ J_{sat} [%]
PM6:BDTN-BF	22.3	20.2	19.3	90.6	86.6
PM6:BDTN-Th	18.0	8.2	7.8	45.6	43.4

a) Under the condition of the short-circuit.

b) Under the condition of the maximal power output.

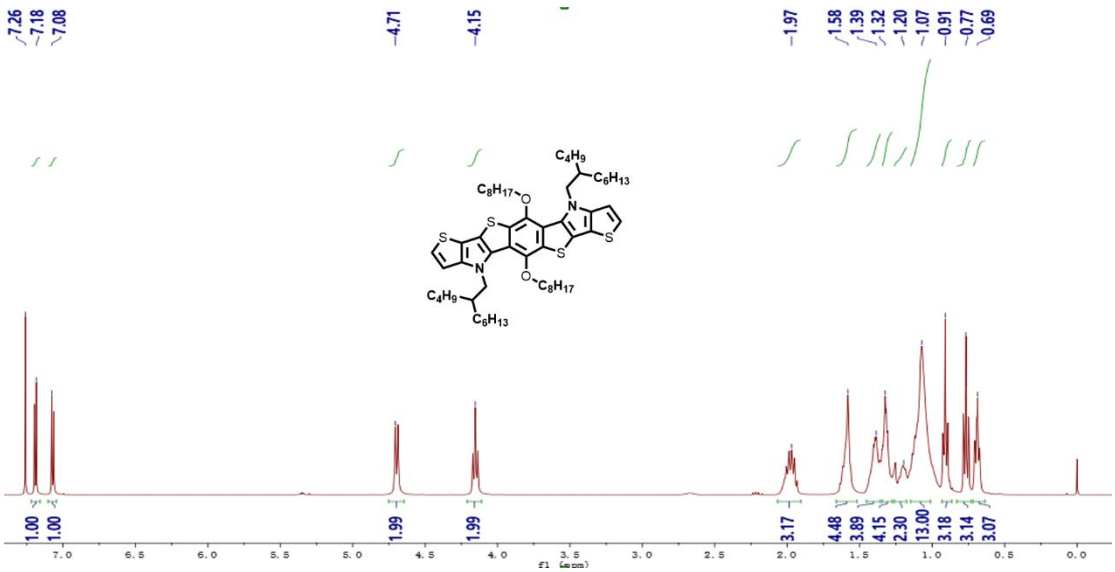

Figure S9. ^{1}H NMR spectrum for BDTN.

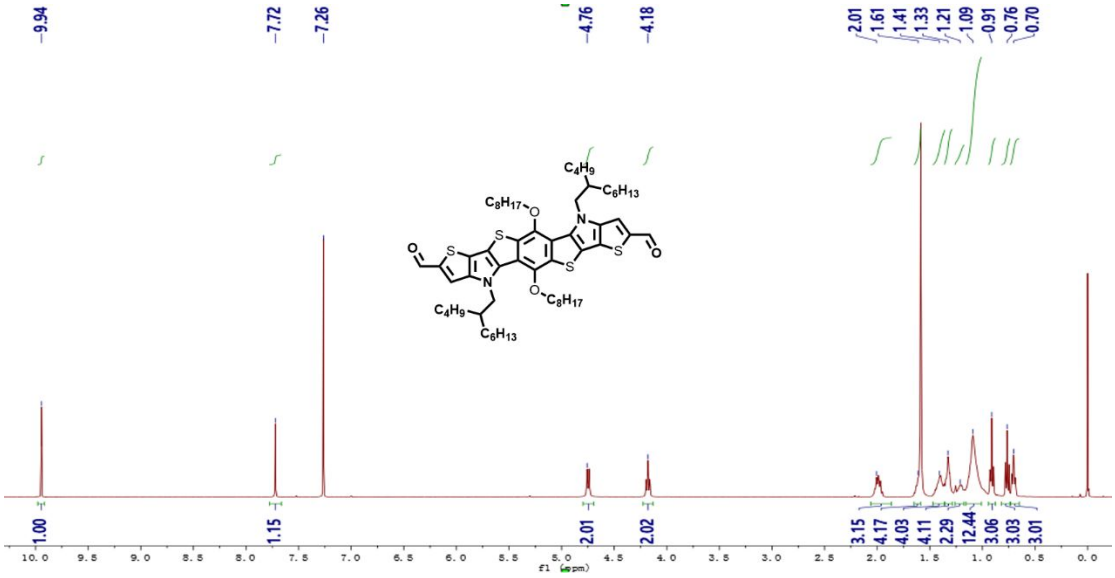

Figure S10.^{1}H NMR spectrum for BDTN-CHO.

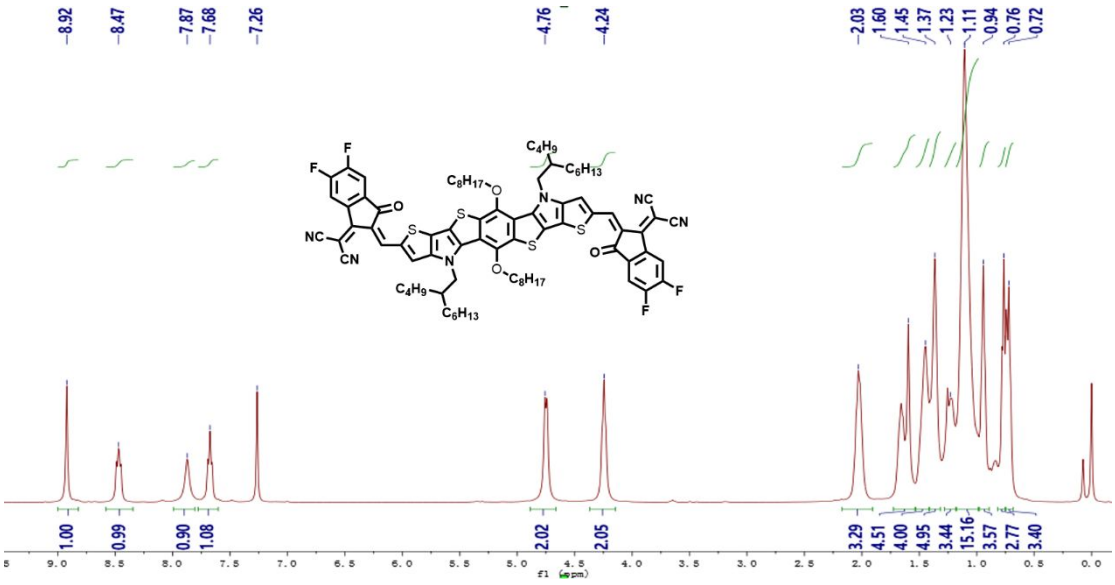

Figure S11.^{1}H NMR spectrum for BDTN-BF.

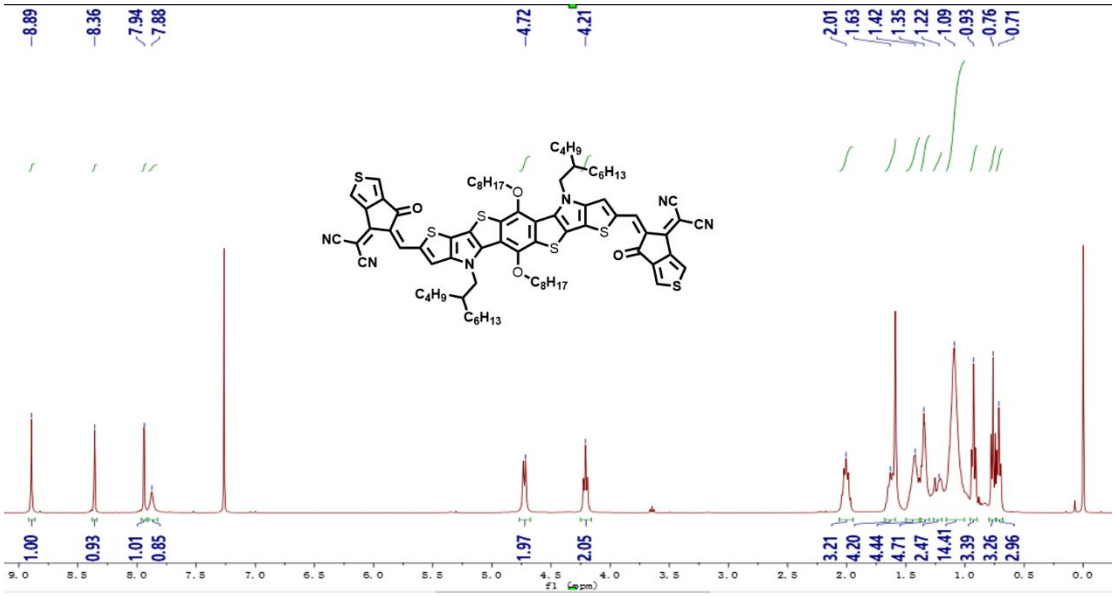

Figure S12.^{1}H NMR spectrum for BDTN-Th.

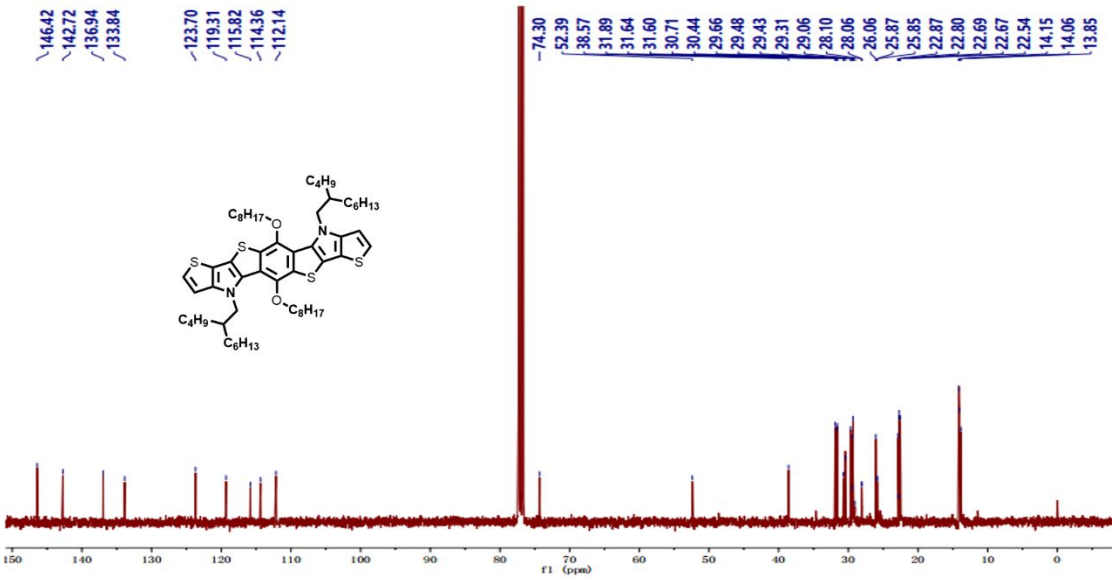

Figure S13.^{13}C NMR spectrum for BDTN.

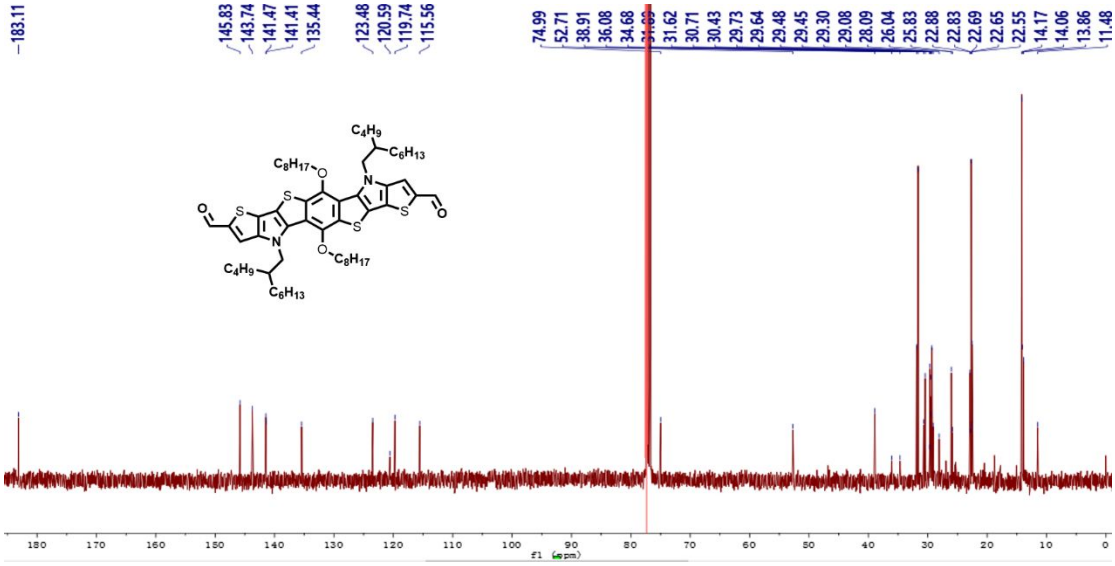

Figure S14. ^{13}C NMR spectrum for BDTN-CHO.

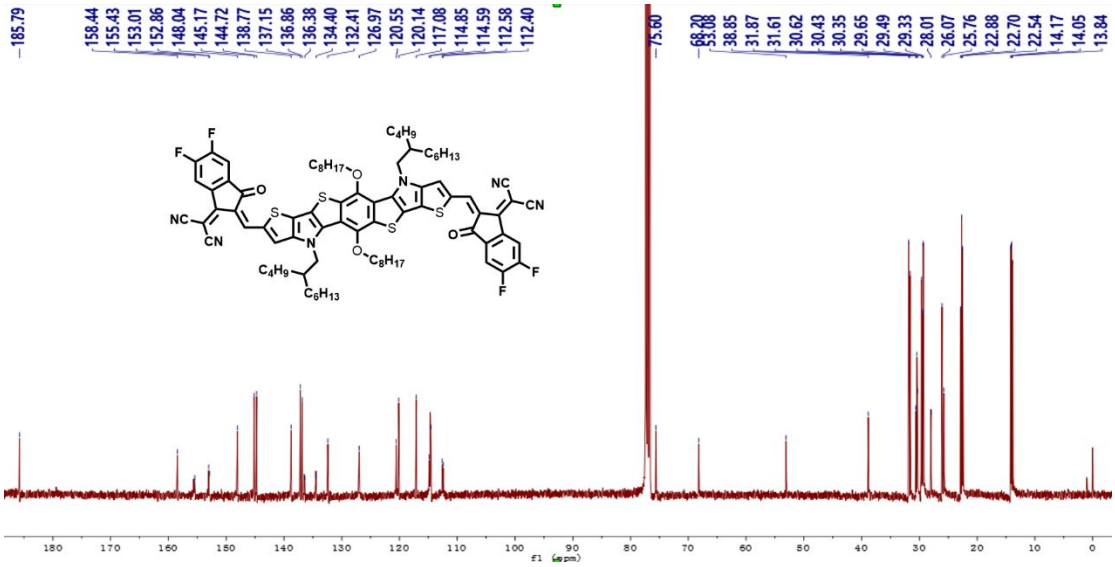

Figure S15. ^{13}C NMR spectrum for BDTN-BF.

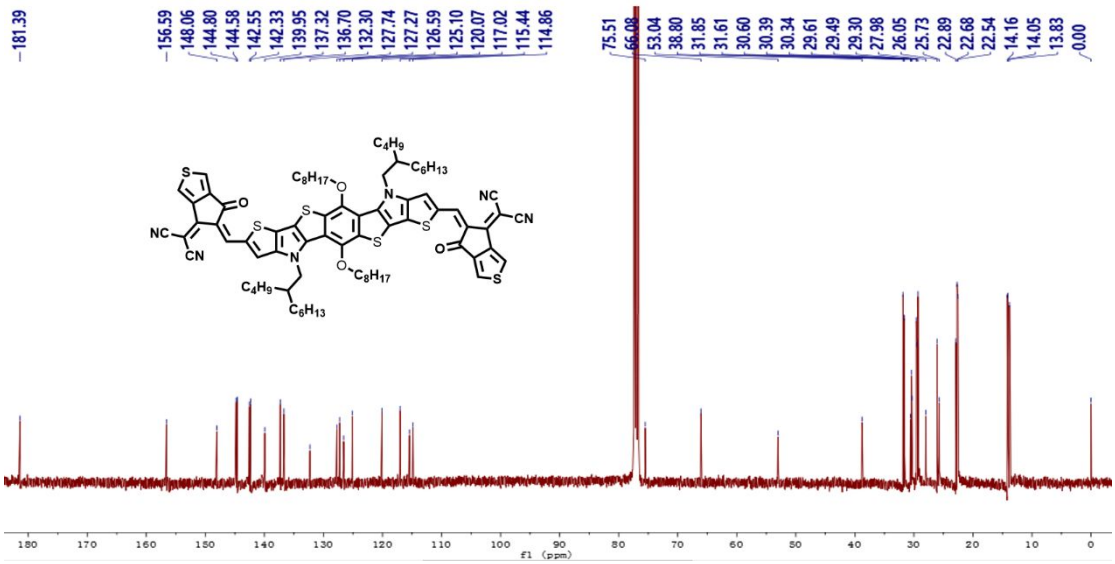

Figure S16. ^{13}C NMR spectrum for BDTN-Th.

References

(1) Kim, Y. J.; Ahn, E. S.; Hwang, M. C.; Park, C. E.; Kim, Y.-H. A Benzodithiophene-Thienothiophene Derivative with Cyano Acrylate Side Chain: A Novel Donor Polymer with Deep HOMO Level for P-N Heterojunction Solar Cells. *Thin Solid Films* **2016**, *603*, 165-172.

(2) Pan, Z.; Liu, Y.; Fan, F.; Chen, Y.; Li, Y.; Zhan, X.; Song, Y. Self-Assembled π-Extended Condensed Benzothiophene Nanoribbons for Field-Effect Transistors. *Chem. Eur. J.* **2013**, *19*, 9771-9774.

(3) Jiang, H.; Oniwa, K.; Xu, Z.; Bao, M.; Yamamoto Y.; Jin, T. Synthesis and Properties of Dicyanomethylene-Endcapped Thienopyrrole-Based Quinoidal S,N-Heteroacenes. *Bull. Chem. Soc. Jpn.* **2017**, *90*, 789-797.

(4) Luo, Z.; Li, G.; Gao, W.; Wu, K.; Zhang, Z.-G.; Qiu, B.; Bin, H.; Xue, L.; Liu, F.; Li, Y.; Yang, C. A Universal Nonfullerene Electron Acceptor Matching with Different Band-Gap Polymer Donors for High-Performance Polymer Solar Cells. *J. Mater. Chem. A* **2018**, *6*, 6874-6881.

(5) Liu, T.; Gao, W.; Wang, Y.; Yang, T.; Ma, R.; Zhang, G.; Zhong, C.; Ma, W.; Yan, H.; Yang, C. Unconjugated Side-Chain Engineering Enables Small Molecular Acceptors for Highly Efficient Non-Fullerene Organic Solar Cells: Insights into the Fine-Tuning of Acceptor Properties and Micromorphology. *Adv. Funct. Mater*. **2019**, *29*, 1902155.

(6) Luo, Z.; Sun, C.; Chen, S.; Zhang, Z.-G.; Wu, K.; Qiu, B.; Yang, C.; Li, Y.; Yang, C., Side-Chain Impact on Molecular Orientation of Organic Semiconductor Acceptors: High Performance Nonfullerene Polymer Solar Cells with Thick Active Layer over 400 nm. *Adv. Energy Mater.* **2018**, *8*, 1800856.

(7) Gao, W.; An, Q.; Zhong, C.; Luo, Z.; Ming, R.; Zhang, M.; Zou, Y.; Liu, F.; Zhang, F.; Yang, C. Designing an Asymmetrical Isomer to Promote the LUMO Energy Level and Molecular Packing of a Non-Fullerene Acceptor for Polymer Solar Cells with 12.6% Efficiency. *Chem. Sci*. **2018**, *9*, 8142-8149.

(8) Xiong, W.; Qi, F.; Liu, T.; Huo, L.; Xue, X.; Bi, Z.; Zhang, Y.; Ma, W.; Wan, M.; Liu, J.; Sun, Y. Controlling Molecular Weight to Achieve High-Efficient Polymer Solar Cells with Unprecedented Fill Factor of 79% Based on Non-Fullerene Small Molecule Acceptor. *Sol. RRL*. **2018**, *2*, 1800129.

(9) Chang, S.-L.; Cao, F.-Y.; Huang, W.-C.; Huang, P.-K.; Huang, K.-H.; Hsu, C.-S.; Cheng, Y.-J. New Thieno[3,2-b]thiophene-Based Acceptor: Tuning Acceptor Strength of Ladder-Type N-Type Materials to Simultaneously Achieve Enhanced V_{oc} and J_{sc} of Nonfullerene Solar Cells. *ACS Energy Lett.* **2018**, *3*, 1722-1729.

(10) Liu, K.-K.; Xu, X.; Wang, J.-L.; Zhang, C.; Ge, G.-Y.; Zhuang, F.-D.; Zhang, H.-J.; Yang, C.; Peng, Q.; Pei, J. Achieving High-Performance Non-Halogenated Nonfullerene Acceptor-Based Organic Solar Cells with 13.7% Efficiency via A Synergistic Strategy of an Indacenodithieno[3,2-B]Selenophene Core Unit and Non-

Halogenated Thiophene-Based Terminal Group. *J. Mater. Chem. A* **2019**, *7*, 24389-24399.

(11) Yang, K.; Liao, Q.; Koh, C. W.; Chen, J.; Su, M.; Zhou, X.; Tang, Y.; Wang, Y.; Zhang, Y.; Woo, H. Y.; Guo, X. Improved Photovoltaic Performance of a Nonfullerene Acceptor Based on a Benzo [B] Thiophene Fused End Group with Extended Π-Conjugation. *J. Mater. Chem. A* **2019**, *7*, 9822-9830.

(12) Luo, Z.; Zhao, Y.; Zhang, Z.-G.; Li, G.; Wu, K.; Xie, D.; Gao, W.; Li, Y.; Yang, C. Side-Chain Effects on Energy-Level Modulation and Device Performance of Organic Semiconductor Acceptors in Organic Solar Cells. *ACS Appl. Mater. Interfaces* **2017**, *9*, 34146-34152.

(13) Xie, D.; Liu, T.; Lee, T. H.; Gao, W.; Zhong, C.; Huo, L.; Luo, Z.; Wu, K.; Xiong, W.; Kim, J. Y.; Choi, H.; Sun, Y.; Yang, C. A New Small Molecule Acceptor Based on Indaceno [2, 1-B: 6, 5-B'] Dithiophene and Thiophene-Fused Ending Group for Fullerene-Free Organic Solar Cells. *Dyes and Pigments* **2018**, *148*, 263-269.

(14) Li, S.; Ye, L.; Zhao, W.; Zhang, S.; Mukherjee, S.; Ade, H.; Hou, J. Energy-Level Modulation of Small-Molecule Electron Acceptors to Achieve over 12% Efficiency in Polymer Solar Cells. *Adv. Mater.* **2016**, *28*, 9423-9429.

(15) Liu, T.; Huo, L.; Chandrabose, S.; Chen, K.; Han, G.; Qi, F.; Meng, X.; Xie, D.; Ma, W.; Yi, Y.; Hodgkiss, J. M.; Liu, F.; Wang, J.; Yang, C.; Sun, Y. Optimized Fibril Network Morphology by Precise Side-Chain Engineering to Achieve High-Performance Bulk-Heterojunction Organic Solar Cells. *Adv. Mater.* **2018**, *30*, 1707353.

(16) Gao, W.; Liu, T.; Ming, R.; Luo, Z.; Wu, K.; Zhang, L.; Xin, J.; Xie, D.; Zhang, G.; Ma, W.; Yan, H.; Yang, C. Near-Infrared Small Molecule Acceptor Enabled High-Performance Nonfullerene Polymer Solar Cells with Over 13% Efficiency. *Adv.*

Funct. Mater. **2018**, *28*, 1803128.

(17) Luo, Z.; Liu, T.; Wang, Y.; Zhang, G.; Sun, R.; Chen, Z.; Zhong, C.; Wu, J.; Chen, Y.; Zhang, M.; Zou, Y.; Ma, W.; Yan, H.; Min, J.; Li, Y.; Yang, C. Reduced Energy Loss Enabled by a Chlorinated Thiophene-Fused Ending-Group Small Molecular Acceptor for Efficient Nonfullerene Organic Solar Cells with 13.6% Efficiency. *Adv. Energy Mater.* **2019**, *9*, 1900041.

(18) Gao, W.; Liu, T.; Luo, Z.; Zhang, L.; Ming, R.; Zhong, C.; Ma, W.; Yan, H.; Yang, C. Regulating Exciton Bonding Energy and Bulk Heterojunction Morphology in Organic Solar Cells via Methyl-Functionalized Non-Fullerene Acceptors. *J. Mater. Chem. A* **2019**, *7*, 6809-6817.

(19) Lin, Y.; Zhao, F.; Prasad, S. K.; Chen, J.; Cai, W.; Zhang, Q.; Chen, K.; Wu, Y.; Ma, W.; Gao, F.; Tang, J.; Wang, C.; You, W.; Hodgkiss, J. M.; Zhan, X. Balanced Partnership between Donor and Acceptor Components in Nonfullerene Organic Solar Cells with> 12% Efficiency. *Adv. Mater.* **2018**, *30*, 1706363.

(20) Kan, B.; Zhang, J.; Liu, F.; Wan, X.; Li, C.; Ke, X.; Wang, Y.; Feng, H.; Zhang, Y.; Long, G.; Friend, R. H.; Bakulin, A. A.; Chen, Y. Fine-Tuning the Energy Levels of a Nonfullerene Small-Molecule Acceptor to Achieve a High Short-Circuit Current and a Power Conversion Efficiency over 12% in Organic Solar Cells. *Adv. Mater.* **2018**, *30*, 1704904.

(21) Xu, S. j.; Zhou, Z.; Liu, W.; Zhang, Z.; Liu, F.; Yan, H.; Zhu, X. A Twisted Thieno[3,4-b]thiophene-Based Electron Acceptor Featuring a 14-π-Electron Indenoindene Core for High-Performance Organic Photovoltaics. *Adv. Mater.* **2017**, *29*, 1704510.

(22) Zhu, J.; Ke, Z.; Zhang, Q.; Wang, J.; Dai, S.; Wu, Y.; Xu, Y.; Lin, Y.; Ma, W.; You, W.; Zhan, X. Naphthodithiophene-Based Nonfullerene Acceptor for

High-Performance Organic Photovoltaics: Effect of Extended Conjugation. *Adv. Mater.* **2018**, *30*, 1704713.

(23) Liu, W.; Zhang, J.; Zhou, Z.; Zhang, D.; Zhang, Y.; Xu, S.; Zhu, X. Design of a New Fused-Ring Electron Acceptor with Excellent Compatibility to Wide-Bandgap Polymer Donors for High-Performance Organic Photovoltaics. *Adv. Mater.* **2018**, *30*, 1800403.

(24) Zhao, W.; Li, S.; Yao, H.; Zhang, S.; Zhang, Y.; Yang, B.; Hou, J. Molecular Optimization Enables over 13% Efficiency in Organic Solar Cells. *J. Am. Chem. Soc.* **2017**, *139*, 7148-7151.

(25) Li, S.; Ye, L.; Zhao, W.; Yan, H.; Yang, B.; Liu, D.; Li, W.; Ade, H.; Hou, J. A Wide Band Gap Polymer with a Deep Highest Occupied Molecular Orbital Level Enables 14.2% Efficiency in Polymer Solar Cells. *J. Am. Chem. Soc.* **2018**, *140*, 7159-7167.

(26) Liu, Y.; Li, M.; Zhou, X.; Jia, Q.; Feng, S.; Jiang, P.; Xu, X.; Ma, W.; Li, H.; Bo, Z. Nonfullerene Acceptors with Enhanced Solubility and Ordered Packing for High-Efficiency Polymer Solar Cells. *ACS Energy Lett.* **2018**, *3*, 1832-1839.